Supplemental Materials

Supplemental Methods

Cell lines and primary cell culture. Primary, normal lung epithelial cells (LE1 and LE2) were obtained and cultured as previously described (1). In brief, normal lung tissue was obtained from the non-cancerous marginal portion of resected lung lobes of NSCLC patients and promptly transported aseptically in Hanks' Balanced Salt Solution (Invitrogen) supplemented with 100 U/mL penicillin, 100 mg/mL streptomycin and 5 mg/mL gentamycin (Invitrogen), followed by incubation with 1.5 U/mL Dispase (Roche) at 4°C overnight. After enzymatic hydrolysis, tissues were dissected, incubated with trypsin (Invitrogen) and resuspended in keratinocyte serum-free medium (KSFM) supplemented with 40 mg/mL Bovine Pituitary Extract (BPE), 1.0 ng/mL epidermal growth factor (EGF), 100 U/mL penicillin, 100 mg/mL streptomycin, 5 mg/mL gentamycin and 100 U/mL nystatin (Invitrogen), and after two weeks of culture, the lung epithelial cells were obtained in KSFM. The Beas2B immortalized human bronchial epithelial cell line (Shanghai Institutes of Biological Sciences) was cultured in LHC-9 medium as instructed by the supplier (Invitrogen). Lung cancer cell lines, including A549, Calu-3, NCI-H1299, PC9 and 95D were obtained from Cell Banks of Shanghai Institutes of Biological Sciences (Shanghai, China), or Fu Erbo Biotechnology Co., Ltd. (Guangzhou, China), and maintained in Dulbecco's Modified Eagle's Medium (DMEM; Invitrogen) supplemented with 10% HyClone Fetal Bovine Serum (FBS) and 1% penicillin/streptomycin (Invitrogen). All cell lines were authenticated by short tandem repeat (STR) fingerprinting at the Forensic Medicine Laboratory of Sun Yat-Sen University (Guangzhou, China) (2).

Colony Formation Assay. Cells were plated in 6-well plates (5×10^2 cells per well)

and cultured in DMEM supplemented with 10% FBS for 10 days. The colonies were stained with 1% crystal violet for 5 minutes after 30 seconds fixation with 4% formaldehyde.

Three-dimension spheroid invasion assay. Cells (1×10^4) were mixed with 20% Matrigel and seeded in 24-well plates coated with 100% Matrigel (BD, Franklin Lakes, NJ), and medium was changed every other day. Three independent experiments were performed.

Sphere formation assays. Five hundred cells were seeded in 6-well ultra-low cluster plates for 10 days. Spheres were cultured in DMEM/F12 serum-free medium (Invitrogen) supplemented with 2% B27 (Invitrogen), 20 ng/ml EGF, 20 ng/ml bFGF (PeproTech), 0.4% BSA (Sigma-Aldrich), and 5 μg/ml insulin.

Flow cytometric analysis. Cells were dissociated with trypsin and resuspended at 1×10^6 cells per milliliter in DMEM containing 2% FBS and then preincubated at 37°C for 30 minutes with or without 100 μM verapamil (Sigma-Aldrich) to inhibit ABC transporters. The cells were subsequently incubated for 90 minutes at 37°C with 5 μg/ml Hoechst 33342 (Sigma-Aldrich), followed by a final incubation on ice for 10 minutes and wash with ice-cold PBS before flow cytometric analysis. Cytometric analysis was performed using the BD Influx flow cytometer with BD FACS Software (BD Biosciences).

Anoikis Assays. For anoikis assays, polyHEMA-coated dishes were prepared by applying 2 ml polyHEMA solution (20 mg/ml polyhydroxyethylmethacrylate, Sigma-Aldrich Co., Milwaukee, WI, USA in ethanol) onto the 60mm dish, drying in a tissue culture hood, followed by one repetition of the above procedure and subsequent by extensive wash with PBS (>3 times) before 10^6 cells were seeded into the prepared

60mm polyHEMA-coated dishes. After 48-hour culture, cells were collected by pipetting. For DNA content analysis, collected cells were fixed, stained with propidium iodide, and analyzed using EPICS XL-MCL flow cytometer with EXPO32 ADC software (Beckman Coulter).

RNA extraction, reverse transcription (RT) and qPCR. Total RNA of cultured cells was extracted using the Trizol reagent (Invitrogen) by following the manufacturer's instruction. cDNA was amplified and quantified on the CFX-1000 qRT-PCR Detection System (Bio-Rad), using the FastStart Universal SYBR Green Master (Roche).

Plasmid construction. Human and mouse TGF-β1 genes were cloned into the pMSCV-neo retroviral vector (Clontech). Human CCT6A was cloned into the pSin EF2 puro lentiviral vector (Addgene). shRNA constructs respectively targeting human SMAD2, SMAD3, CCT6A and mouse Smad2, Smad3, Cct6a were cloned into the pSuper-retro-puro retroviral vector (Oligoengine). Modified firefly luciferase gene Luc2 was cloned into the pMSCV-hygro retroviral vector. SMAD1, 2, 3, 4, 5, 8, SAMD2 pseudo-phosphorylation mutant, truncated SMAD2 fragments and HA-tagged CCT6A were cloned into the pCDNA3.1 plasmid (Invitrogen). All primers and oligonucleotides are listed in Table S1.

Immunohistochemistry (IHC). Paraffin-embedded NSCLC serial sections were analyzed using IHC with antibodies against p-SMAD2 (1:100), p-SMAD3 (1:100), TGF-β (1:100), CCT6A (1:200), APC (1:100), DKK3 (1:50) and Frizzled1 (1:100), respectively. To quantify the expression level of each protein, the mean optical density (OD) of protein staining in each section was calculated from 3 randomly picked 200× magnified frames. "High" and "Low" expression of each protein was

stratified using the median OD among all patients' cases as the cut-off value. All antibodies are listed in Table S2.

Table S1. Primers and Oligonucleotides

Flag-Tagged SMAD2 and SMAD2 fragments (AA, amino acid residue)

	Forward Primer	Reverse Primer
SMAD2	gccggtaccgccatggactacaaggacgacga tgacaagtcgtccatcttgccattcac	ggcgaattctcatgacatgcttgagcaacgcac
SMAD2 AA 1-172	gccggtaccgccatggactacaaggacgacga tgacaagtcgtccatcttgccattcac	ggcgaattctcatgtctcaactctctgatagtggt
SMAD2 AA 173-267	gccggtaccatggactacaaggacgacgatga caagccagttttgcctccagtattagt	ggcgaattctcaaactggctgtaaatccaagctat
SMAD2 AA 268-467	gccggtaccatggactacaaggacgacgatga caagacttactcagaacctgcattttg	ggcgaattctcatgacatgcttgagcaacgcac

SMAD pseudo phosphorylation mutation

	Forward Primer	Reverse Primer
SMAD2 S2D mut.	ccagtgtgatggatatctgcagaattctcagtcca tgtctgagcaacgcactgaagggg	ccccttcagtgcgttgctcagacatggactgagaattctg cagatatccatcacactgg
SMAD3 S2D mut	tcctcacccagatgggctccccaagcatccgctg ttccgatgtggattag	ctaatccacatcggaacagcggatgcttggggagccca tctgggtgagga

Flag-Tagged SMADs

	Forward Primer	Reverse Primer
SMAD1	gccggtaccgccatggactacaaggacgacga tgacaagaatgtgacaagtttattttc	ggcggatcctcaagatacagatgaaataggattatg
SMAD3	gccggatccgccatggactacaaggacgacga tgacaagtcgtccatcctgcctttcac	ggcgaattctcaagacacactggaacagcggatg
SMAD4	gccggatccgccatggactacaaggacgacga tgacaaggacaatatgtctattacgaa	ggcgaattctcagtctaaaggttgtgggtctgc
SMAD5	gccggtaccgccatggactacaaggacgacga tgacaagacgtcaatggccagcttgttttcttttac	ggcggatcctcatgaaacagaagatatggggttcagag ggg

SMAD8	gccggatccgccatggactacaaggacgacga tgacaagcactccaccacccccatcag	ggcgaattctcaagacactgaagaaatggggttatg

HA-Tagged CCT6A

	Forward Primer	Reverse Primer
HA-CCT6A	gccggtaccgccatgtacccatacgacgtccca gactacgctgcggcggtgaagaccct	ggcggatcctcaacctttcagagaagacattccagc

pMSCV-Puro-TGFB1

	Forward Primer	Reverse Primer
TGFB1	gccagatctgccatgccgccctccgggctgcgg	ggcgaattctcagctgcacttgcaggagcg

pMSCV-Puro-Tgfb1

	Forward Primer	Reverse Primer
Tgfb1	gccagatctatgccgccctcggggctgcggcta ctgccg	ggcgaattctcagctgcacttgcaggagcgcacaatca tg

Oligonucleotides used for shRNAs (Sense Sequence)

Gene	Oligonucleotide
CCT6A-1	gctggagacatcaaactta
CCT6A-2	tgtcattagagtatgagaa
SMAD2-1	gtcccatgaaaagacttaa
SMAD2-2	ggattgccacatgttatat
SMAD3-1	ggagaaatggtgcgagaag

SMAD3-2	ggacgaggtctgcgtgaat
Cct6a	gcagggcttgtctatgagtat
Smad2	cctaagtgatagtgcaatctt
Smad3	cccatgtttctgcatggattt

Primers used for qPCR

	Forward Primer	Reverse Primer
FZD1	cagcacagcactgaccaaat	gtgagccgaccaaggtgtat
FZD4	tcttctctgtgcacattggc	gacaactttcacaccgctca
FZD5	gagagacggttagggctcg	gtgacccagggacggag
FZD7	gtcgtgtttcatgatggtgc	cgcctctgttcgtctacctc
FZD8	gacacgaagaggtagcaggc	caccgtctccaccttcctta
EZH2	ctgattttacacgcttccgc	ggaacaacgcgagtcgg
BMI1	tcgttgttcgatgcatttct	ctttcattgtcttttccgcc
RPL13	tggccagtttcagttcttca	tgaaggagtaccgctccaaa
RPL18	atatcctggctcttgggctc	acctggccgagcaggag
RPS3	tcctcggagtttcccagac	tcctaggagggcttgctgt
RPS9	cagcttcatcttgccctcat	ctgctgacgcttgatgagaa
APC	tcttcagtgcctcaacttgc	ggagacagaatggaggtgct
DKK3	caggtgtactggaagctggc	tcacatctgtgggagacgaa

WIF1	ggacattgacggttggatct	tgaattttacctggcaagctg
CDKN1C	tggcgaagaaatcggagat	caggagcctctcgctgac
SFTPB	cagcactttaaaggacggtgt	gggtgtgtgggaccatgt
DNAI2	atggtgccatacacagggtc	tggctgctacaatggacaga
FABP6	ggctgcttaggccagtctct	ctcagagatcgtgggtgaca

Table S2.

Antibodies used for WB and IHC

Antibody name	Manufacture	Cat. number
SMAD2	Cell Signaling Technology	#5339
SMAD3	Abcam	ab28379
p-SMAD2	Cell Signaling Technology	#3108
p-SMAD3	Abcam	ab52903
H3K4me3	Abcam	ab8580
Flag Tag	Sigma-Aldrich	F7425
HA Tag	Sigma-Aldrich	H3663
CCT6A	Aviva	OAAF04361
SMAD4	Abcam	ab3219
SMAD5	Abcam	ab40771
TGF-β	Abcam	ab66043
APC	Bethyl	A300-979A
DKK3	Abcam	ab2459
Frizzled1	Sigma-Aldrich	F3804

Supplemental Reference

1. Ibrahim L, Dominguez M, Yacoub M. Primary human adult lung epithelial cells in vitro: response to interferon-gamma and cytomegalovirus. Immunology. 1993;79:119-24.
2. Butler JM. Forensic DNA typing : biology, technology, and genetics of STR markers. 2nd ed. ed. London: Elsevier Academic Press; 2005.

Supplementary Figure Legends

Supplementary Figure S1. NSCLC metastasis is associated with inactivation of SMAD2-mediated and activation of SMAD3-mediated transcriptional programs.

(A) Heat map of ChIP enrichment signal surrounding SMAD2 and SMAD3 peaks shows chromosomal distribution of SMAD2 and SMAD3 in indicated Calu3 cells. **(B)** Venn diagram shows the overlapping status of SMAD2 and SMAD3 occupied enhancers in A549 and Calu3 cells. **(C)** Western blot show the efficiency and specificity of shRNAs knockdown of SMAD2 and SMAD3 in A549 and Calu3 cells. Representative images derived from 3 independent experiments. **(D)** Average binding density profile of SMAD2, SMAD3 and H3K4me3 around SMAD2 and SMAD3 peaks center in TGF-β treated A549 and Calu3 cells. **(E)** Microarray-based transcription profiling shows that silencing SMAD2 or SMAD3 significantly attenuates the transactivation of genes distinctly regulated by these two SMADs, and to a lesser extent attenuates their shared target transcripts, when induced by TGF-β. Box and whiskers plots represent the mRNA levels. Data were analyzed by Student's *t* test. $^{**}P < 0.01$. **(F)** Gene Set Enrichment analysis (GSEA) analysis (Upper panel) and Kaplan-Meier analysis (Lower panel) show that decreased SMAD2 specific- and increased SMAD3 specific-transcripts are presented in NSCLC patients with higher metastatic potential and associated with shorter metastasis-free survival in patients enrolled in the MSKCC NSCLC dataset 2, whereas targets shared by SMAD2 and SMAD3 are not associated with metastasis status. "High" and "Low" expression of each gene set was stratified by the median of normalized expression level among all genes of the set.

Supplementary Figure S2. TGF-β-induced metastasis of NSCLC is suppressed

by SMAD2 and promoted by SMAD3.

(A-I) Luciferase living image of mice at different time points following intravenous (via tail vein) injection of indicated NSCLC cells (A), and the mice living image of day 30 are also shown in Figure 2 A and C. Kaplan-Meier survival analysis of mice intravenously (via tail vein) injected with indicated NSCLC cells (B). Luciferase live-cell imaging (C and E), picric acid staining of metastatic foci and H&E staining of lung tissue (D and F), area percentage of tumor metastatic foci per field (G) and Kaplan-Meier survival analysis (H) of mice with intravenously (via tail vein) injected the indicated NSCLC cells (shRNA set2 of SMAD2 and SMAD3). Representative images were from 2 independent experiments with 6 mice per group with similar results. Error bars represent the means ± SD of 3 independent experiments. *P* values were obtained from ANOVA with Dunnett's *t*-test, $^{**}P < 0.01$. Scale bar: 100 μm. (I) Immunohistochemical staining of p-SMAD2 and p-SMAD3 proteins in paraffin sections of the indicated xenografts. Scale bar: 100 μm. **(J-L)** Luciferase living image of mice at different time points following subcutaneous injection of indicated NSCLC cells in the inguinal folds (J) and the mice living image of day 40 were also shown in Figure 2 E and G. The area percentage of tumor metastatic foci per field (K) and Kaplan-Meier survival analysis (L) of mice subcutaneously injected with indicated NSCLC cells into inguinal folds. Representative images were from 2 independent experiments with 6 mice per group with similar results. *P* values were obtained by performing ANOVA with Dunnett's *t*-test, $^{**}P < 0.01$. **(M-O)** Luciferase live-cell imaging (M), picric acid staining of metastatic foci (N) and Kaplan-Meier survival analysis (O) of C57BL/6 mice intravenously (via tail vein) injected with indicated LLC cells. Representative images were from 2 independent experiments with 6 mice per group with similar results.

Supplementary Figure S3. SMAD2 mediates a tumor-suppressive transcriptional program, whereas SMAD3 mediates a pro-cell survival transcriptional program, in NSCLC cells.

(A) Bar chart presents enriched gene ontology (GO) terms in target genes distinctly specific for, or commonly shared by, SMAD2 and SMAD3. **(B)** Venn Diagram show representative targets distinctly specific for, or commonly shared by, SMAD2 and SMAD3. **(C)** ChIP enrichment plot show the enrichment of SMAD2 and SMAD3 in their corresponding specific or shared target genes in A549 and Calu3 cells. **(D)** 3D culture assays performed in indicated cells. The representative image derived from 3 independent experiments. Scale bar: 100 μm. **(E)** Flow cytometry analysis of Hoechst 33342 dye exclusion (SP+ cell proportions) in indicated cells. The representative image derived from 3 independent experiments. **(F)** Flow cytometer analysis of sub-G1 population of cells grown in polyHEMA-coated plates for 48h. The representative image derived from 3 independent experiments. **(G)** Western blot shows the efficiency and specificity of shRNAs targeting SMAD2 and SMAD3 in indicated cells. The representative image derived from 3 independent experiments. **(H)** Western blot shows that expression of SMAD2 and SMAD3 as well as their phosphorylation status following TGF-β stimulation, does not exhibit significant differences among primarily cultured lung epithelial cells (LE1/2), immortalized bronchial epithelial cells (Beas2B), low-metastatic (A549, Calu3) and highly-metastatic (PC9, 95D) NSCLC cells. The representative images derived from 3 independent experiments.

Supplementary Figure S4. CCT6A specifically interacts with SMAD2 and suppresses the SMAD2-mediated transcriptional program.

(A) Mass spectrum plot of representative peptides from indicated proteins identified

to be SMAD2- or SMAD3-specific or their shared interacting partners. **(B)** Endogenous IP assays performed in Beas2B and A549 cells, which showed that endogenous SMAD2 and CCT6A interacted with each other specifically, but not with other R-SMADs (SMAD3 and SMAD5). The representative images derived from 3 independent experiments. (**C)** Western blot shows the efficiency of overexpressing or knocking down CCT6A in indicated cells. The representative images derived from 3 independent experiments.

Supplementary Figure S5. CCT6A promotes NSCLC cell survival and blocks the SMAD2-SMAD4 interaction.

(A) 3D culture assays performed in indicated cells. The representative images derived from 3 independent experiments. Scale bar: 100 μm. **(B)** Flow cytometry analysis of Hoechst 33342 dye exclusion (SP+ cell proportions) showed that overexpressing CCT6A elevates side population in A549 cells, whereas silencing CCT6A reduces side population in PC9 cells. The representative images derived from 3 independent experiments. **(C)** Flow cytometer analysis of sub-G1 population of cells grown in polyHEMA-coated plates for 48h. The representative images derived from 3 independent experiments. **(D)** Western blots performed in Beas2B and A549 cells with or without HA-CCT6A ectopic expression and TGF-β treatment. The representative image derived from 3 independent experiments. **(E)** Immunofluorescence staining of SMAD2, SMAD3 and HA-CCT6A in Beas2B and A549 cells with or without HA-CCT6A ectopic expression and TGF-β treatment. The representative images derived from 3 independent experiments.

Supplementary Figure S6. CCT6A mediates TGF-β-promoted metastasis of NSCLC cells.

(A-K) Luciferase living image of mice at different time points following intravenously (via tail vein) injecting indicated NSCLC cells (A) and the mice living image of day 30 are also shown in Figure 6 A and C. Kaplan-Meier survival analysis of mice intravenously (via tail vein) injected with indicated NSCLC cells (B). Luciferase live-cell imaging (C and G), picric acid staining of metastatic nodes and H&E staining of lung tissue (D and H), area percentage of tumor metastatic foci per field (E and I) and Kaplan-Meier survival analysis (F and J) of mice with intravenously (via tail vein) injected the indicated NSCLC cells (CCT6A shRNA set2 and SMAD2 shRNA). Representative images were from 2 independent experiments with 6 mice per group with similar results. Error bars represent the means ± SD of 3 independent experiments. *P* values were obtained from ANOVA with Dunnett's *t*-test, $^{**}P < 0.01$. Scale bar: 100 μm. (K) Immunohistochemical staining of p-SMAD2 and p-SMAD3 proteins in paraffin sections of the indicated xenografts. Scale bar: 100 μm. **(L-N)** Luciferase living image of mice at different time points following subcutaneously injecting indicated NSCLC cells into inguinal folds (L) and the mice living image of day 40 are also shown in Figure 6 E and G. The area percentage of tumor metastatic foci per field (M) and Kaplan-Meier survival analysis (N) of mice subcutaneously injected with indicated NSCLC cells into inguinal folds. Representative images were from 2 independent experiments with 6 mice per group with similar results. *P* values were obtained by performing ANOVA with Dunnett's *t*-test, $^{**}P < 0.01$. **(O-Q)** Luciferase live-cell imaging (O), picric acid staining of metastatic foci (P) and Kaplan-Meier survival analysis (Q) of C57BL/6 mice intravenously (via tail vein) injected with indicated LLC cells. Representative images were from 2 independent experiments with 6 mice per group with similar results. **(R, S)** Comparison of the biological outcomes between groups with SMAD2 knocked

down alone and with SMAD2 knocked down plus CCT6A overexpression or knockdown. Kaplan-Meier survival analysis of mice intravenously (via tail vein) injected with indicated NSCLC cells (R) and statistical analyses of colony formation in an adherent culture, tumor sphere formation, sub-G1 DNA content of detached cells and the area percentages of tumor metastatic foci per field were performed in indicated cells (S). Error bars represent means ± SD of 3 independent experiments. *P* values were obtained by performing ANOVA with Dunnett's *t*-test, NS: $P > 0.05$. **(T, U)** Tumor sphere formation assays with indicated NSCLC cells. Error bars represent the means ± SD, *P* values were obtained from Student's *t* test, $*P < 0.05$, $**P < 0.01$.

Supplementary Figure S1

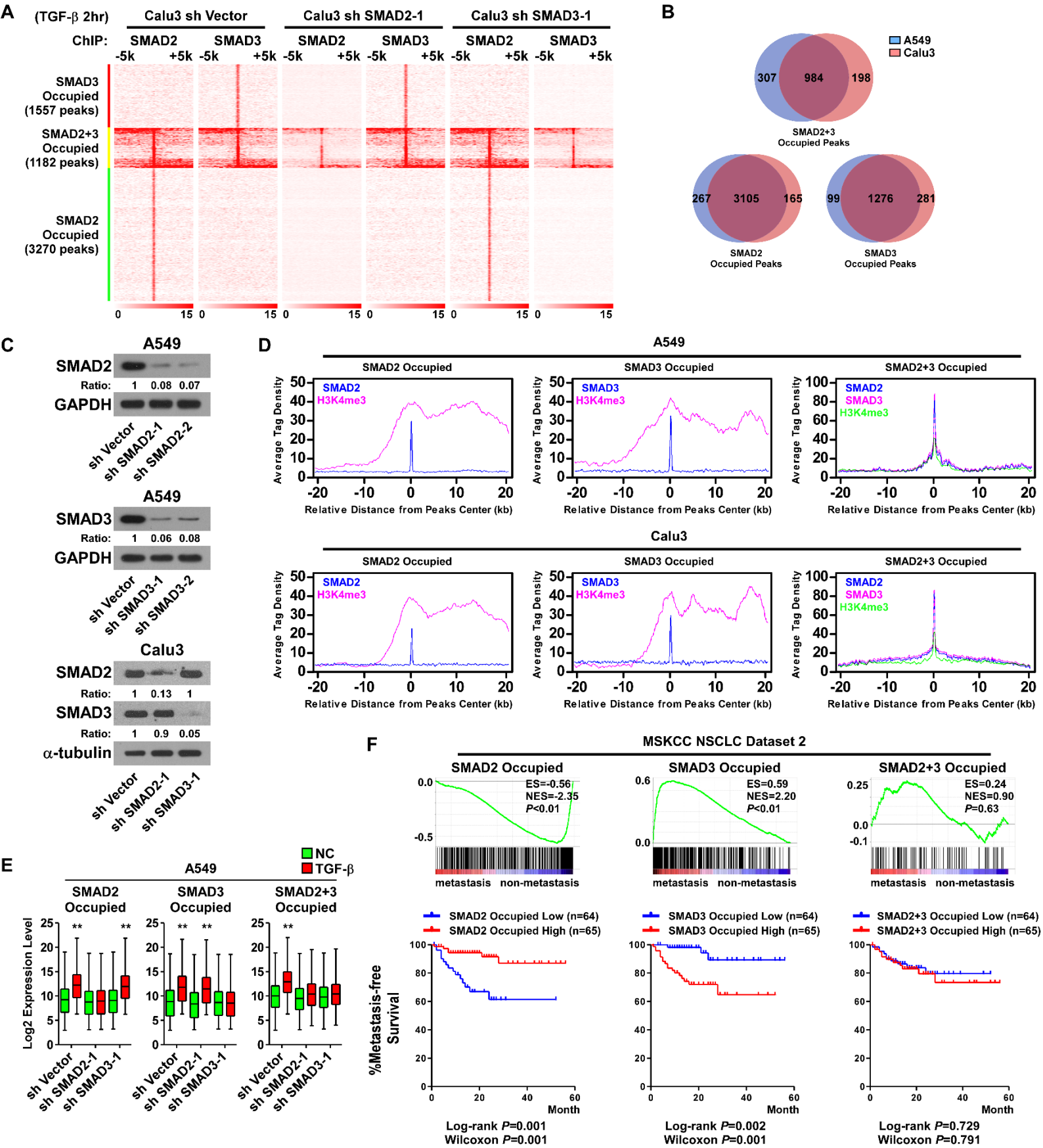

Supplementary Figure S1. NSCLC metastasis is associated with inactivation of SMAD2-mediated and activation of SMAD3-mediated transcriptional programs.

(A) Heat map of ChIP enrichment signal surrounding SMAD2 and SMAD3 peaks shows chromosomal distribution of SMAD2 and SMAD3 in indicated Calu3 cells. **(B)** Venn diagram shows the overlapping status of SMAD2 and SMAD3 occupied enhancers in A549 and Calu3 cells. **(C)** Western blot show the efficiency and specificity of shRNAs knockdown of SMAD2 and SMAD3 in A549 and Calu3 cells. Representative images derived from 3 independent experiments. **(D)** Average binding density profile of SMAD2, SMAD3 and H3K4me3 around SMAD2 and SMAD3 peaks center in TGF-β treated A549 and Calu3 cells. **(E)** Microarray-based transcription profiling shows that silencing SMAD2 or SMAD3 significantly attenuates the transactivation of genes distinctly regulated by these two SMADs, and to a lesser extent attenuates their shared target transcripts, when induced by TGF-β. Box and whiskers plots represent the mRNA levels. Data were analyzed by Student's *t* test. $^{**}P < 0.01$. **(F)** Gene Set Enrichment analysis (GSEA) analysis (Upper panel) and Kaplan-Meier analysis (Lower panel) show that decreased SMAD2 specific- and increased SMAD3 specific-transcripts are presented in NSCLC patients with higher metastatic potential and associated with shorter metastasis-free survival in patients enrolled in the MSKCC NSCLC dataset 2, whereas targets shared by SMAD2 and SMAD3 are not associated with metastasis status. "High" and "Low" expression of each gene set was stratified by the median of normalized expression level among all genes of the set.

Supplementary Figure S2

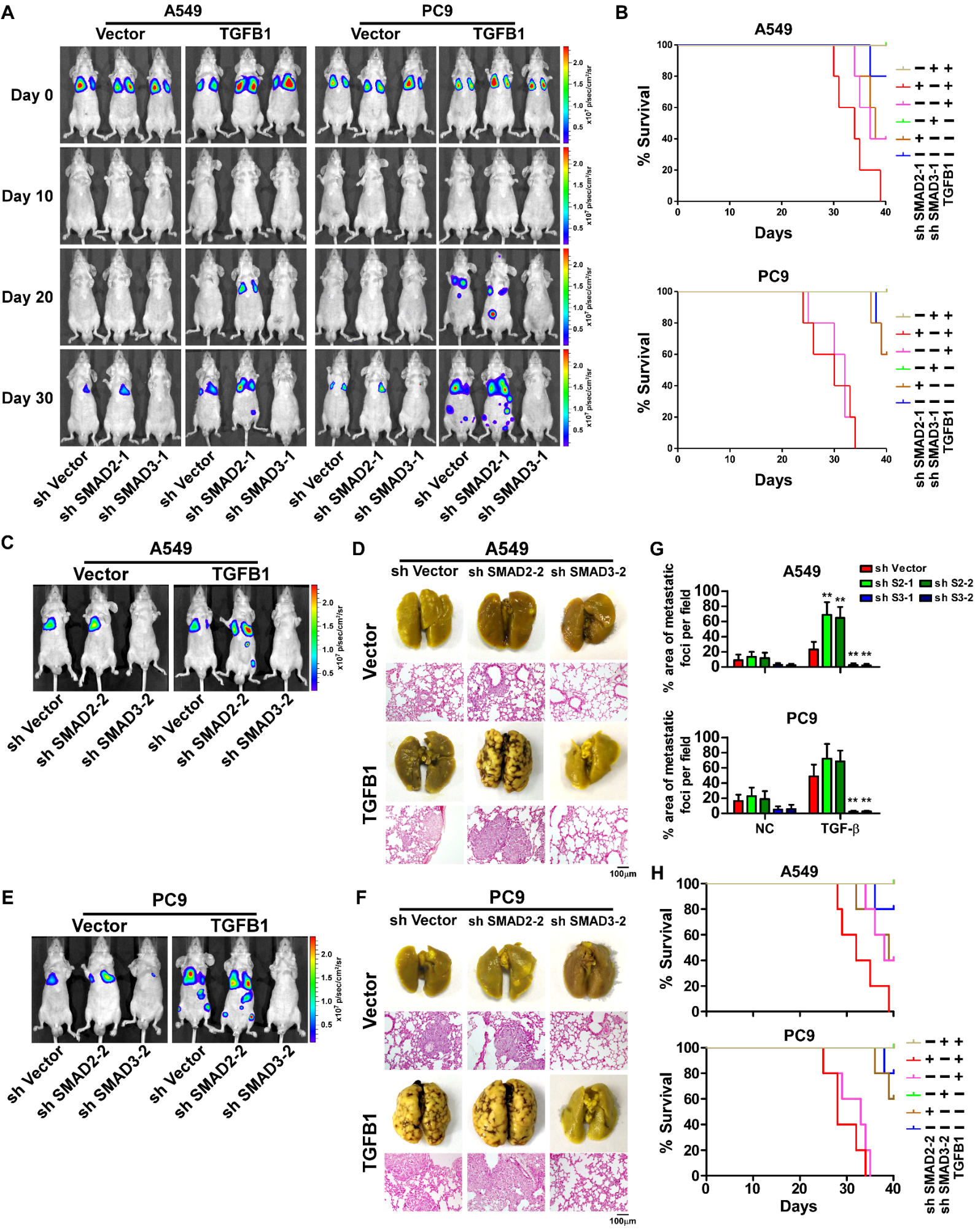

Supplementary Figure S2

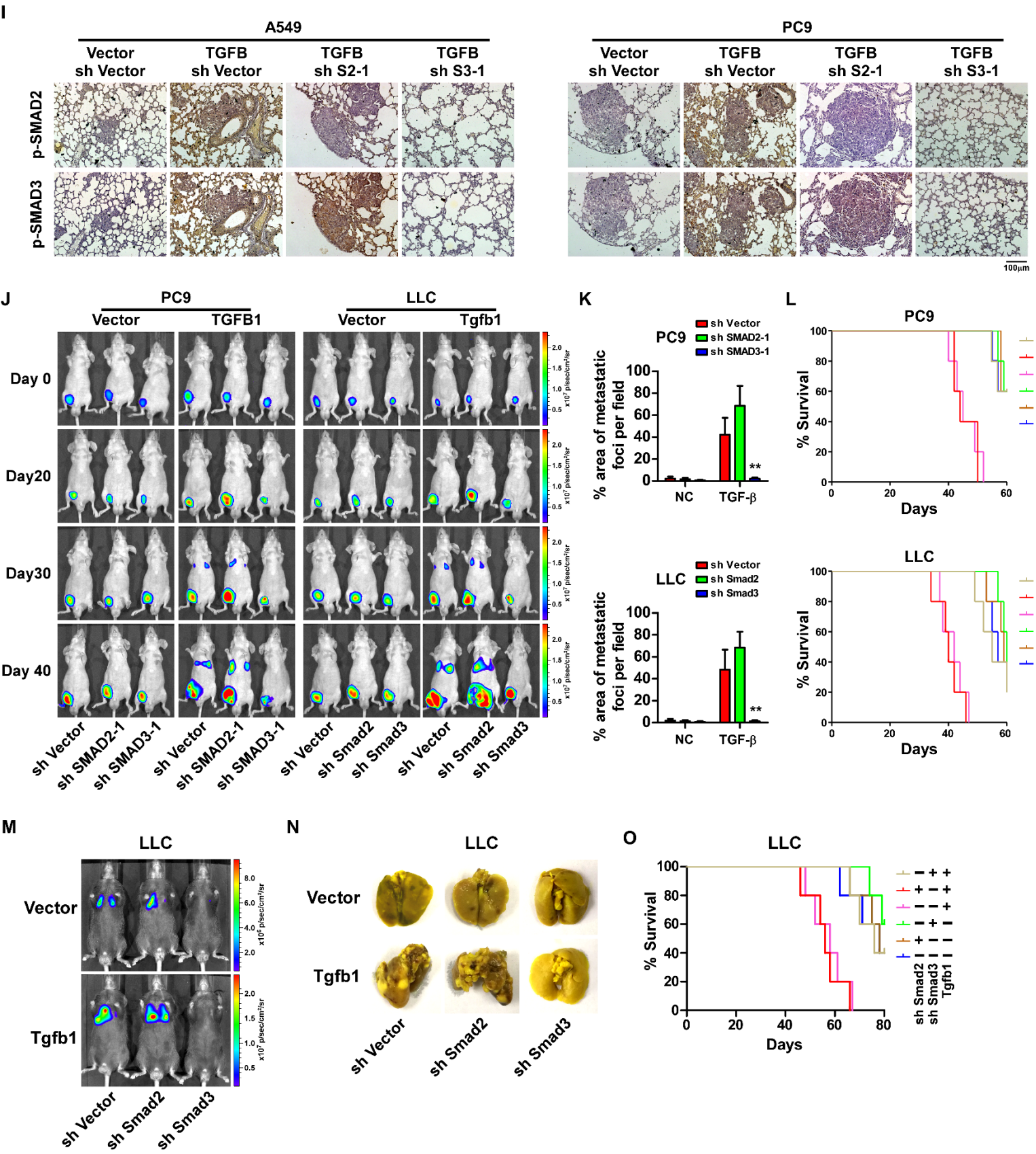

Supplementary Figure S2. TGF-β-induced metastasis of NSCLC is suppressed by SMAD2 and promoted by SMAD3.

(A-I) Luciferase living image of mice at different time points following intravenous (via tail vein) injection of indicated NSCLC cells (A), and the mice living image of day 30 are also shown in Figure 2 A and C. Kaplan-Meier survival analysis of mice intravenously (via tail vein) injected with indicated NSCLC cells (B). Luciferase live-cell imaging (C and E), picric acid staining of metastatic foci and H&E staining of lung tissue (D and F), area percentage of tumor metastatic foci per field (G) and Kaplan-Meier survival analysis (H) of mice with intravenously (via tail vein) injected the indicated NSCLC cells (shRNA set2 of SMAD2 and SMAD3). Representative images were from 2 independent experiments with 6 mice per group with similar results. Error bars represent the means ± SD of 3 independent experiments. *P* values were obtained from ANOVA with Dunnett's *t*-test, $^{**}P < 0.01$. Scale bar: 100 μm. (I) Immunohistochemical staining of p-SMAD2 and p-SMAD3 proteins in paraffin sections of the indicated xenografts. Scale bar: 100 μm. **(J-L)** Luciferase living image of mice at different time points following subcutaneous injection of indicated NSCLC cells in the inguinal folds (J) and the mice living image of day 40 were also shown in Figure 2 E and G. The area percentage of tumor metastatic foci per field (K) and Kaplan-Meier survival analysis (L) of mice subcutaneously injected with indicated NSCLC cells into inguinal folds. Representative images were from 2 independent experiments with 6 mice per group with similar results. *P* values were obtained by performing ANOVA with Dunnett's *t*-test, $^{**}P < 0.01$. **(M-O)** Luciferase live-cell imaging (M), picric acid staining of metastatic foci (N) and Kaplan-Meier survival analysis (O) of C57BL/6 mice intravenously (via tail vein) injected with indicated LLC cells. Representative images were from 2 independent experiments with 6 mice per group with similar results.

Supplementary Figure S3

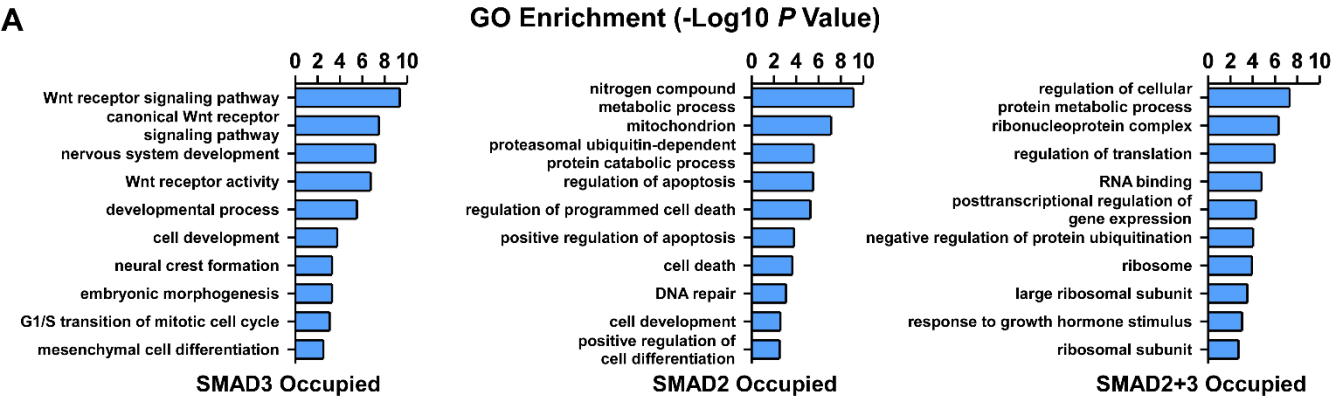

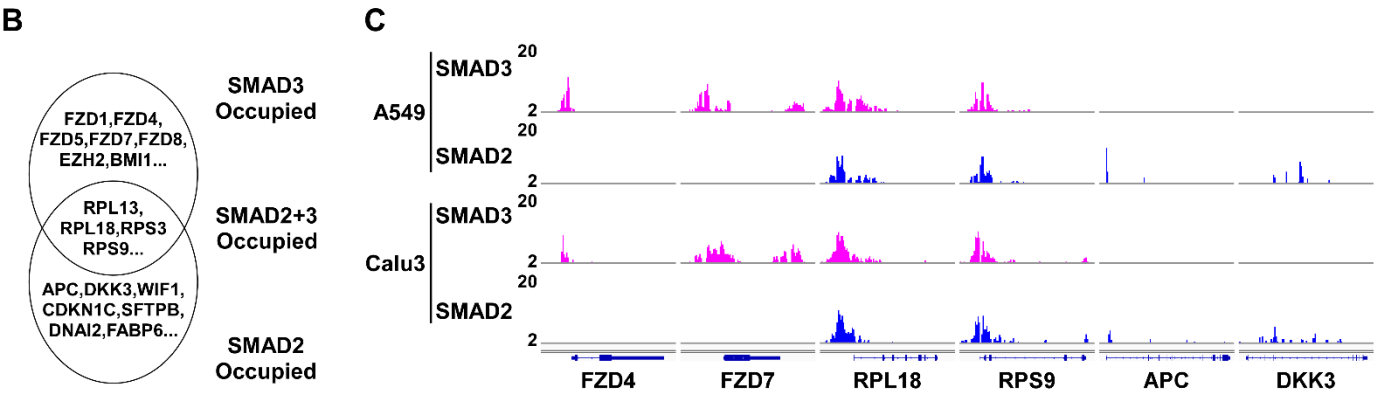

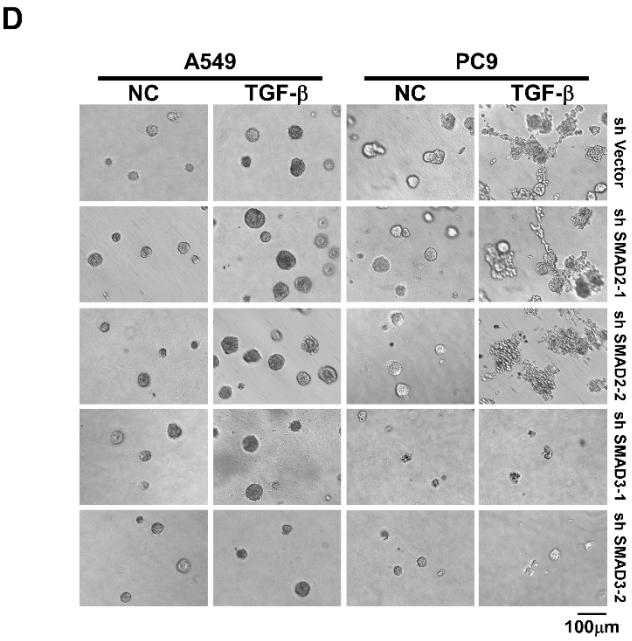

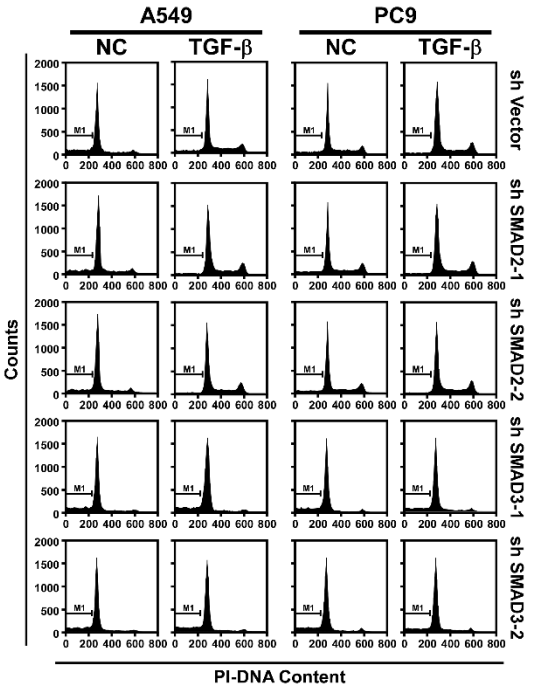

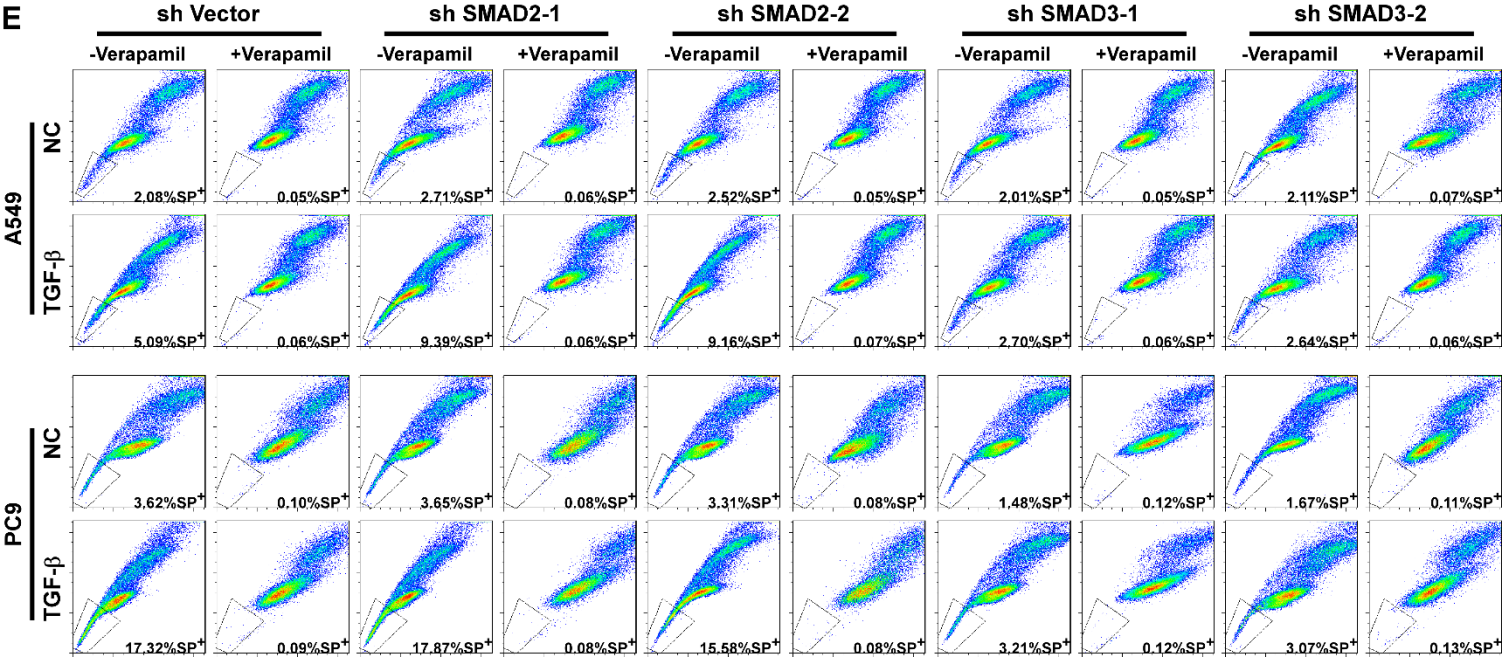

Supplementary Figure S3

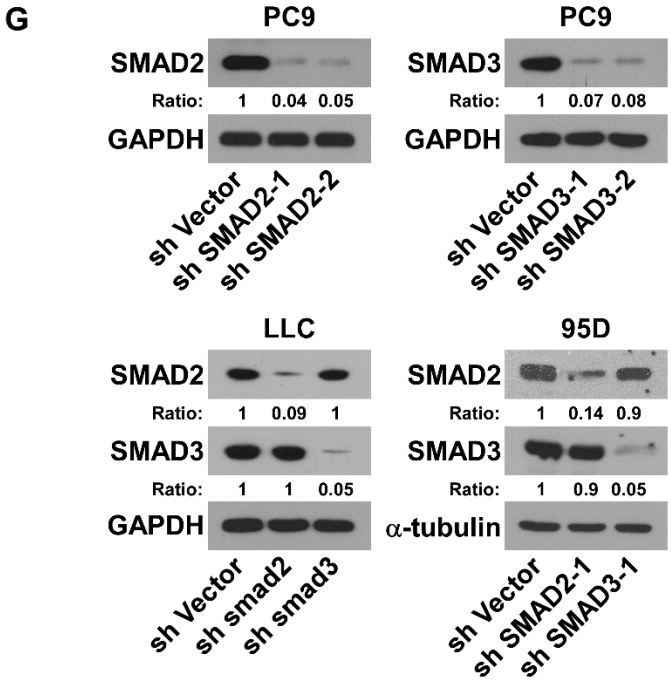

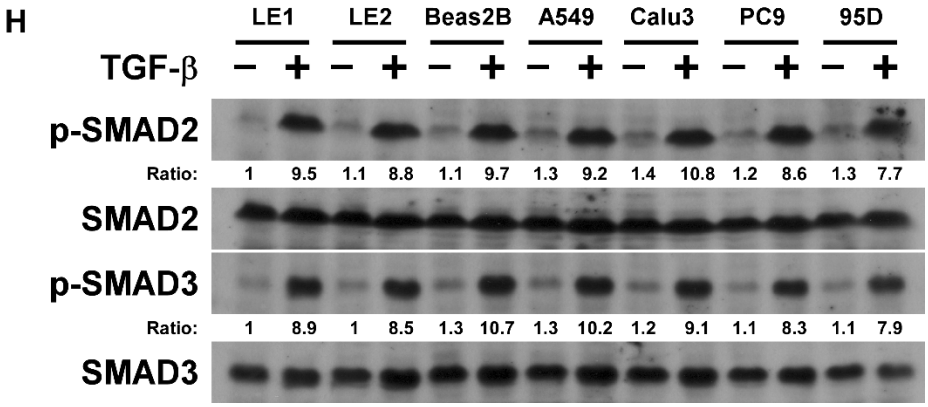

Supplementary Figure S3. SMAD2 mediates a tumor-suppressive transcriptional program, whereas SMAD3 mediates a pro-cell survival transcriptional program, in NSCLC cells.

(A) Bar chart presents enriched gene ontology (GO) terms in target genes distinctly specific for, or commonly shared by, SMAD2 and SMAD3. **(B)** Venn Diagram show representative targets distinctly specific for, or commonly shared by, SMAD2 and SMAD3. **(C)** ChIP enrichment plot show the enrichment of SMAD2 and SMAD3 in their corresponding specific or shared target genes in A549 and Calu3 cells. **(D)** 3D culture assays performed in indicated cells. The representative image derived from 3 independent experiments. Scale bar: 100 μm. **(E)** Flow cytometry analysis of Hoechst 33342 dye exclusion (SP+ cell proportions) in indicated cells. The representative image derived from 3 independent experiments. **(F)** Flow cytometer analysis of sub-G1 population of cells grown in polyHEMA-coated plates for 48h. The representative image derived from 3 independent experiments. **(G)** Western blot shows the efficiency and specificity of shRNAs targeting SMAD2 and SMAD3 in indicated cells. The representative image derived from 3 independent experiments. **(H)** Western blot shows that expression of SMAD2 and SMAD3 as well as their phosphorylation status following TGF-β stimulation, does not exhibit significant differences among primarily cultured lung epithelial cells (LE1/2), immortalized bronchial epithelial cells (Beas2B), low-metastatic (A549, Calu3) and highly-metastatic (PC9, 95D) NSCLC cells. The representative images derived from 3 independent experiments.

Supplementary Figure S4

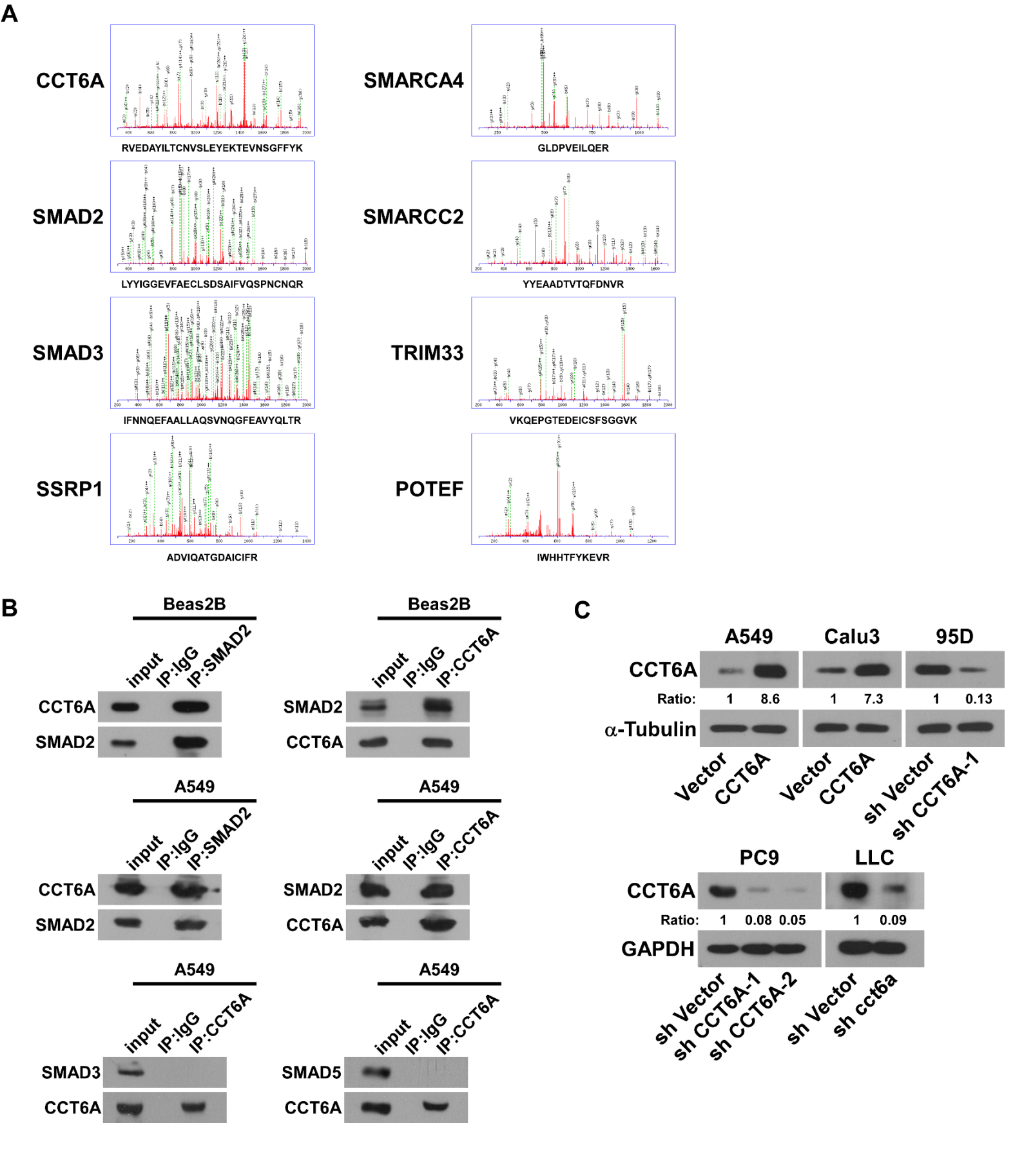

Supplementary Figure S4. CCT6A specifically interacts with SMAD2 and suppresses the SMAD2-mediated transcriptional program.

(A) Mass spectrum plot of representative peptides from indicated proteins identified to be SMAD2- or SMAD3-specific or their shared interacting partners. **(B)** Endogenous IP assays performed in Beas2B and A549 cells, which showed that endogenous SMAD2 and CCT6A interacted with each other specifically, but not with other R-SMADs (SMAD3 and SMAD5). The representative images derived from 3 independent experiments. (**C)** Western blot shows the efficiency of overexpressing or knocking down CCT6A in indicated cells. The representative images derived from 3 independent experiments.

Supplementary Figure S5

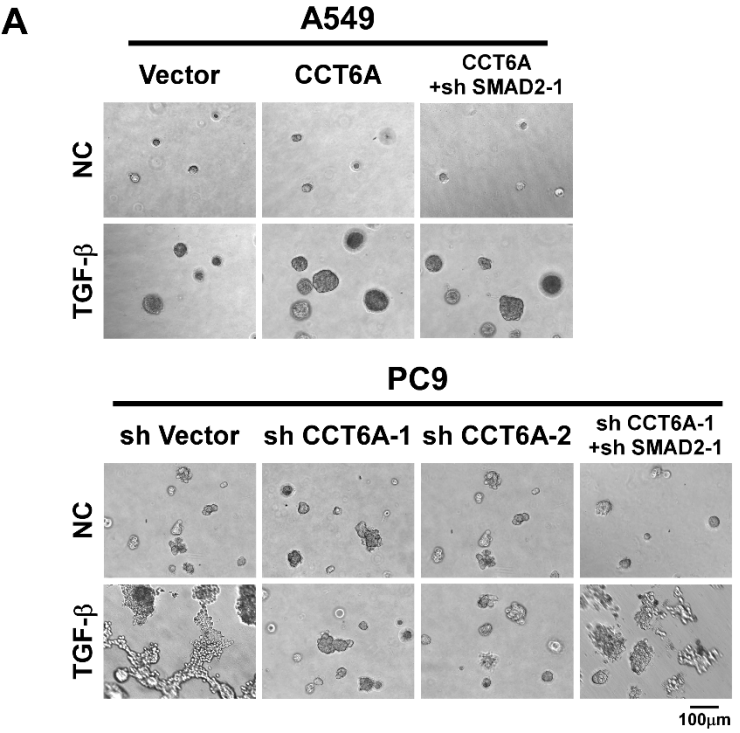

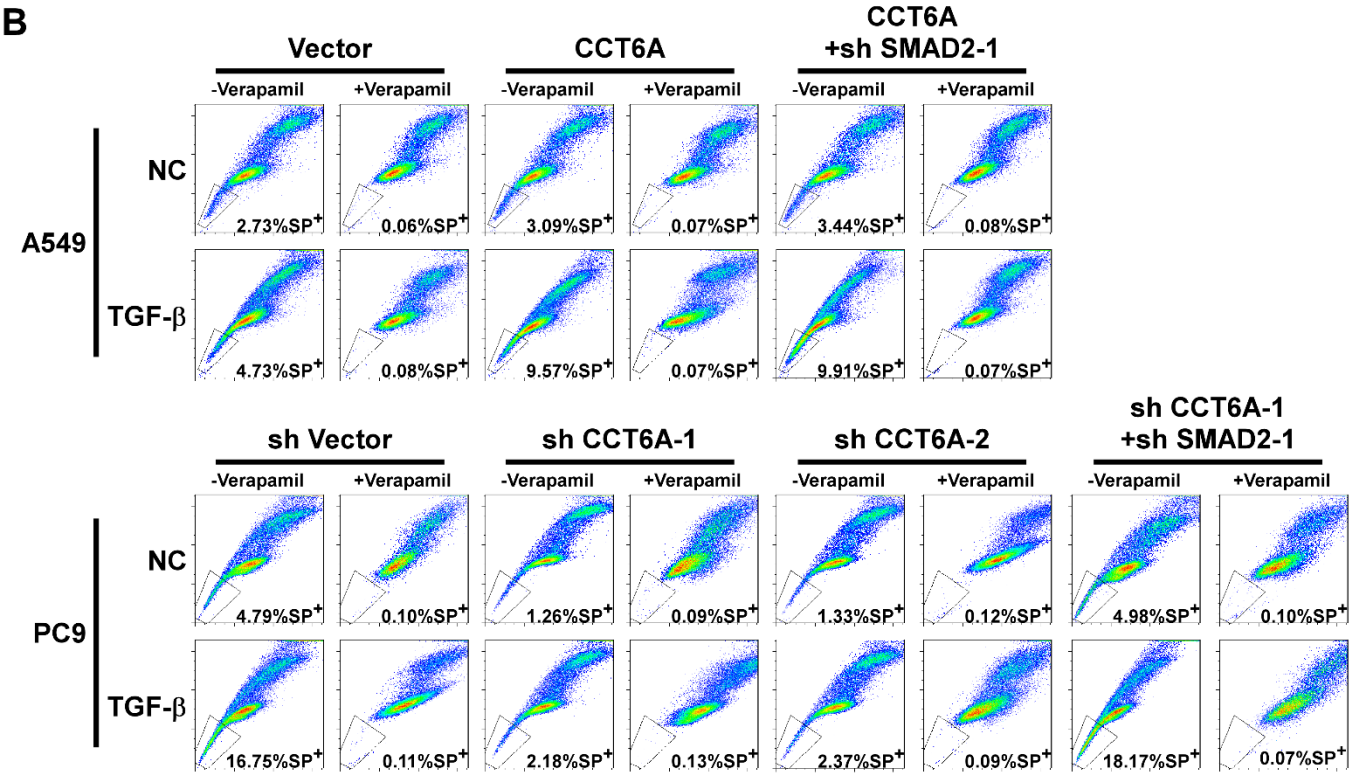

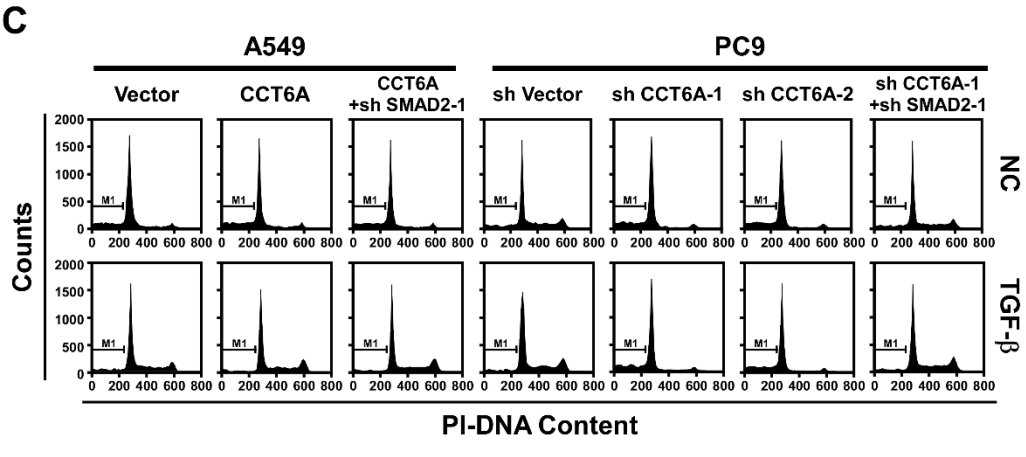

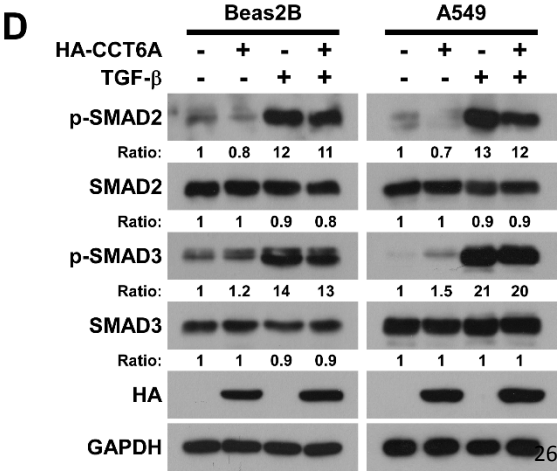

Supplementary Figure S5

E

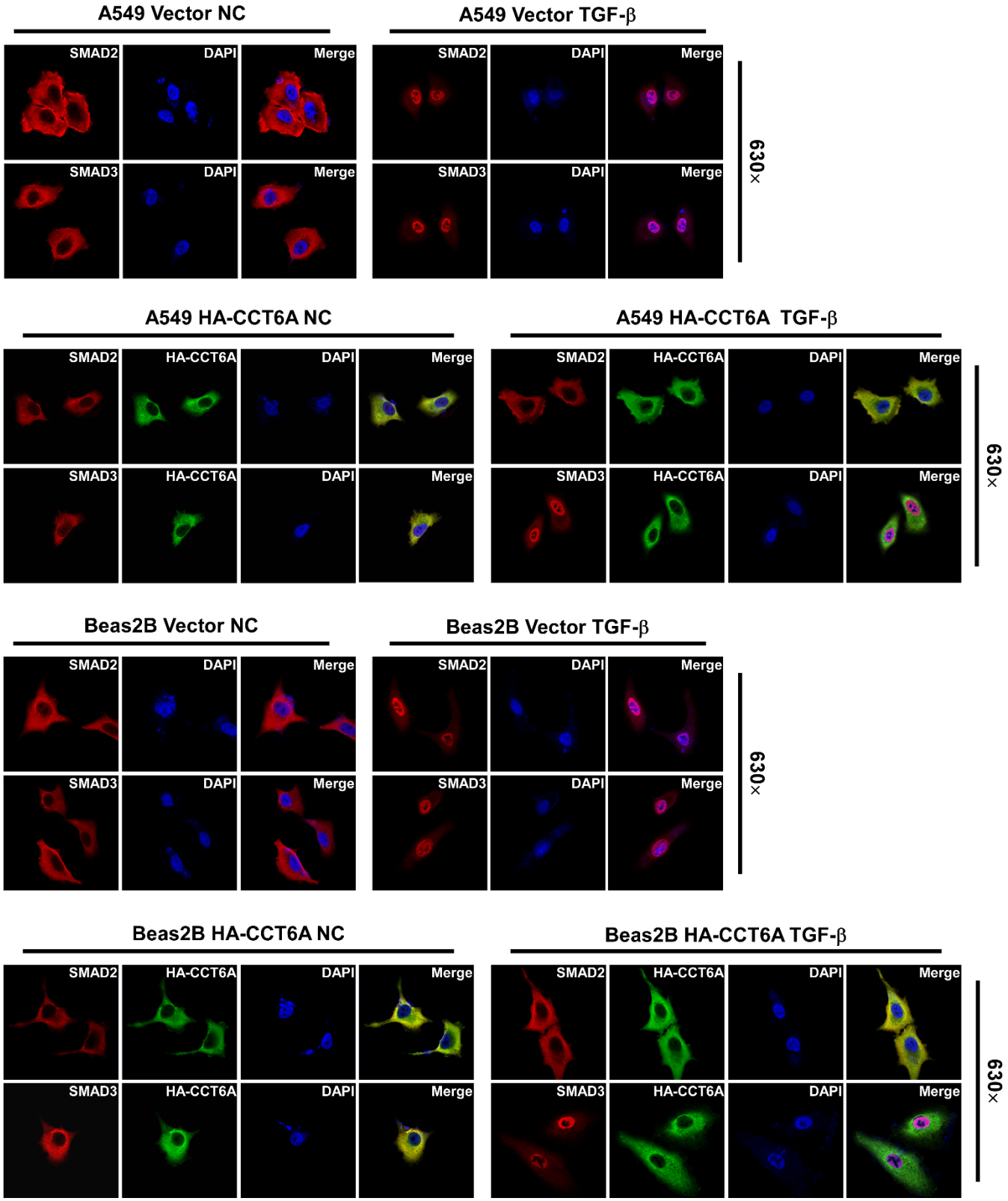

Supplementary Figure S5. CCT6A promotes NSCLC cell survival and blocks the SMAD2-SMAD4 interaction.

(A) 3D culture assays performed in indicated cells. The representative images derived from 3 independent experiments. Scale bar: 100 μm. **(B)** Flow cytometry analysis of Hoechst 33342 dye exclusion (SP+ cell proportions) showed that overexpressing CCT6A elevates side population in A549 cells, whereas silencing CCT6A reduces side population in PC9 cells. The representative images derived from 3 independent experiments. **(C)** Flow cytometer analysis of sub-G1 population of cells grown in polyHEMA-coated plates for 48h. The representative images derived from 3 independent experiments. **(D)** Western blots performed in Beas2B and A549 cells with or without HA-CCT6A ectopic expression and TGF-β treatment. The representative image derived from 3 independent experiments. **(E)** Immunofluorescence staining of SMAD2, SMAD3 and HA-CCT6A in Beas2B and A549 cells with or without HA-CCT6A ectopic expression and TGF-β treatment. The representative images derived from 3 independent experiments.

Supplementary Figure S6

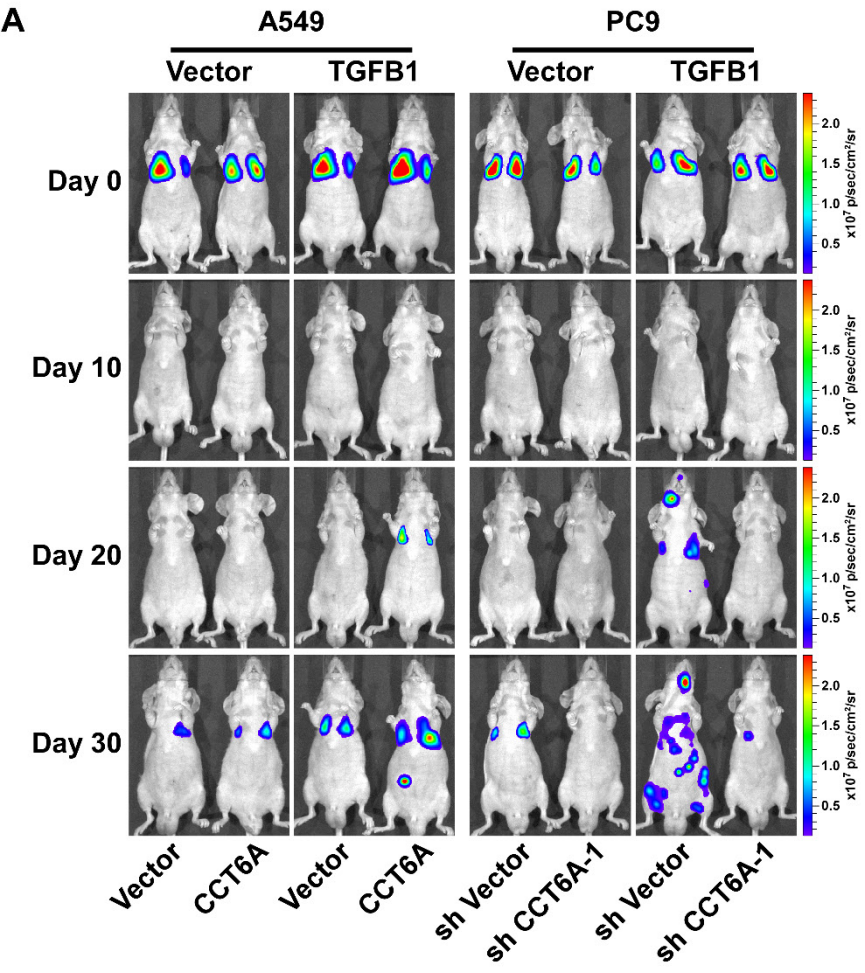

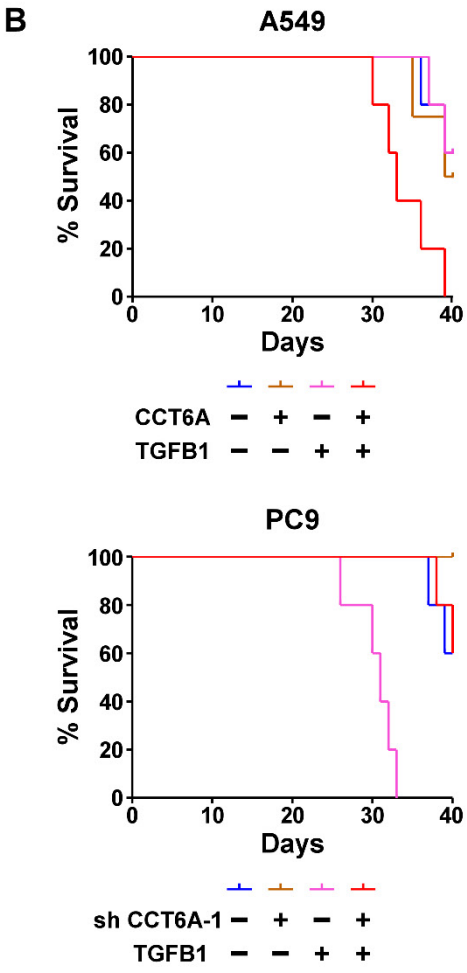

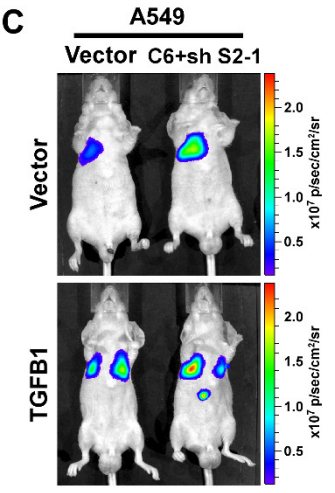

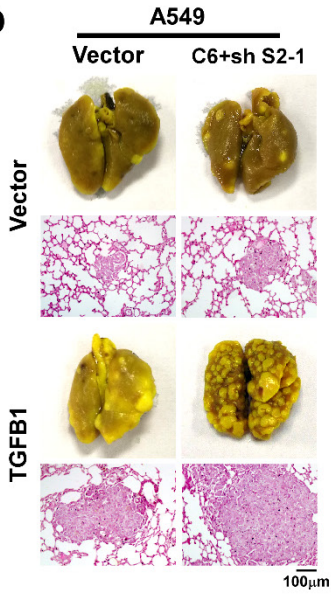

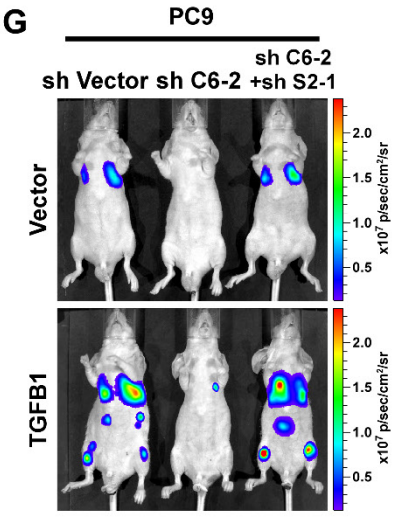

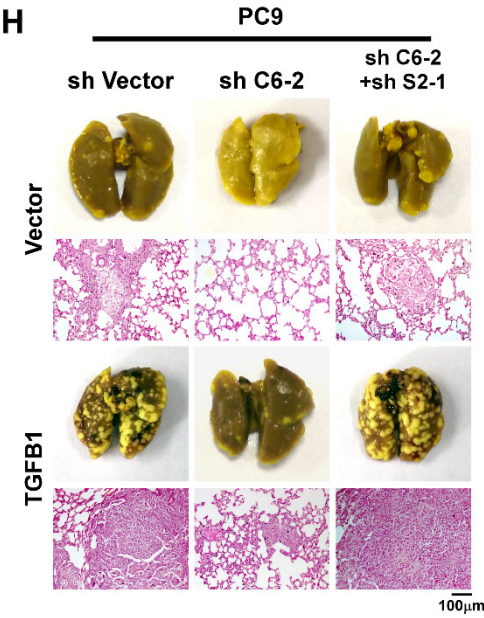

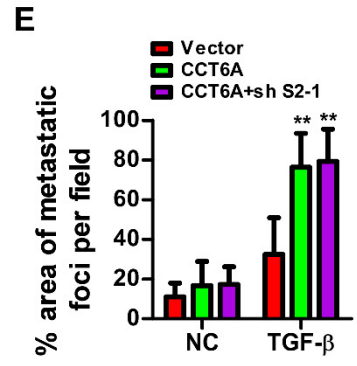

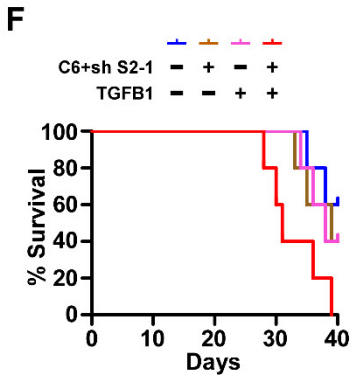

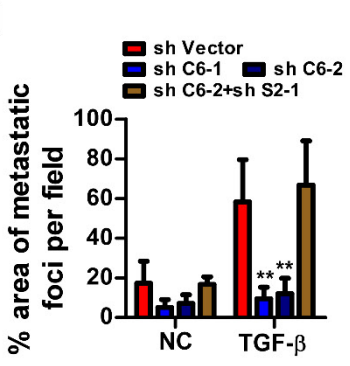

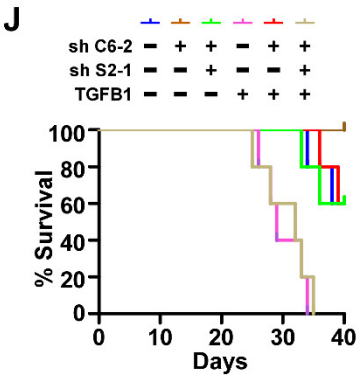

Supplementary Figure S6

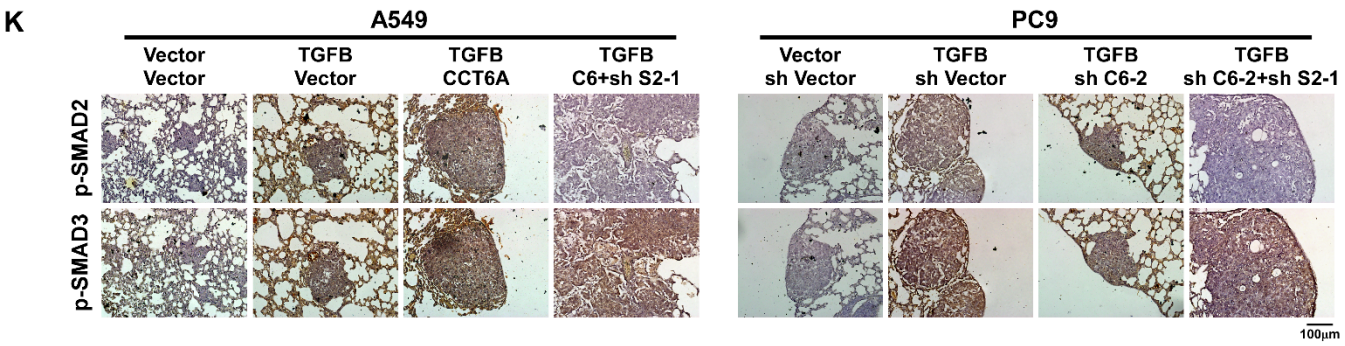

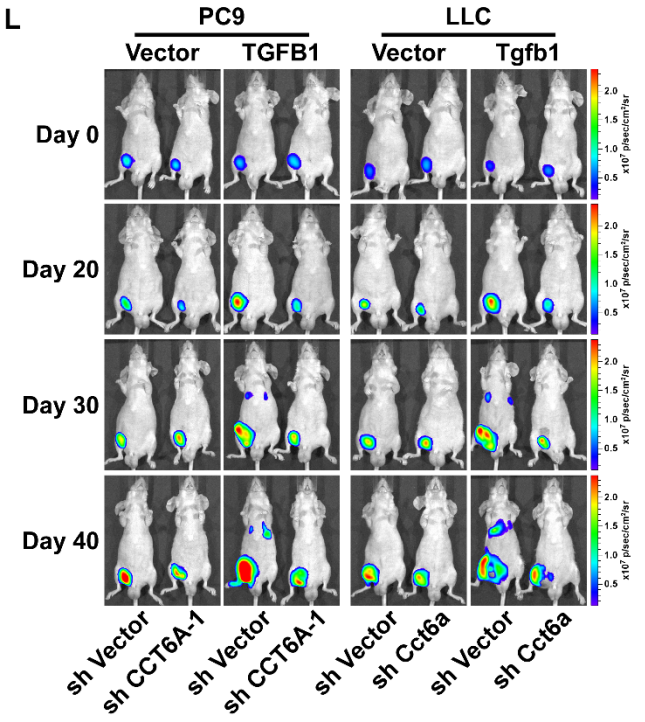

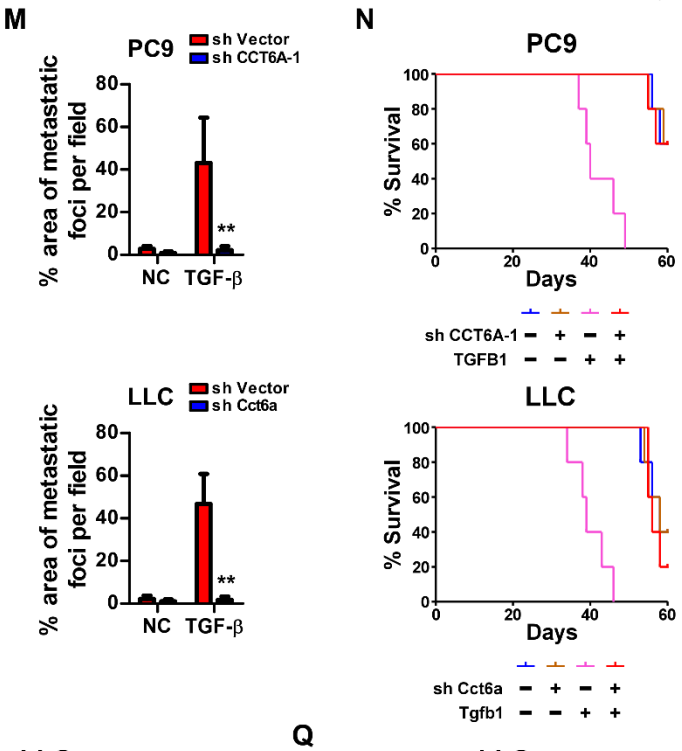

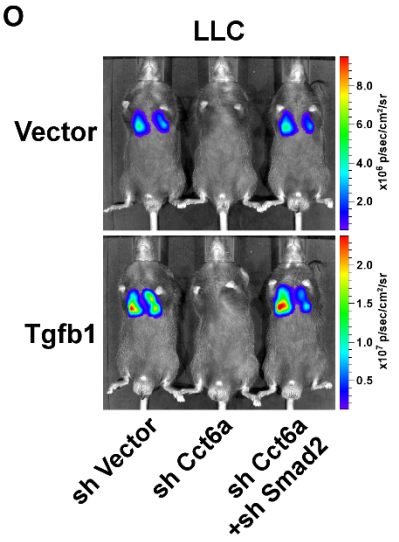

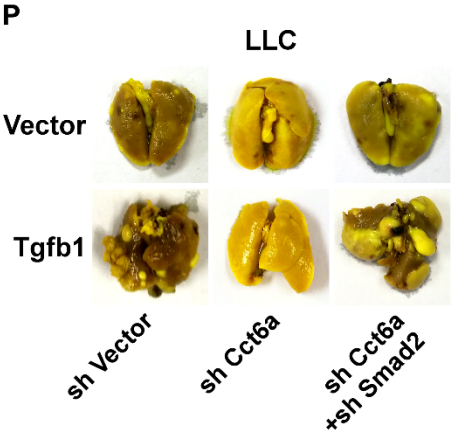

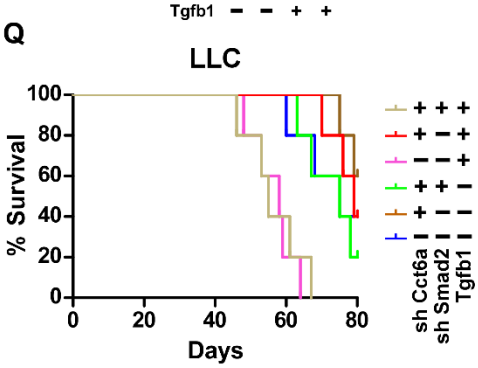

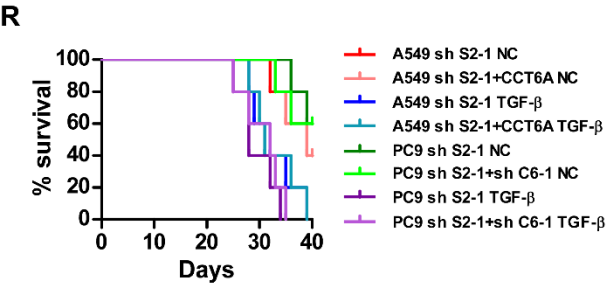

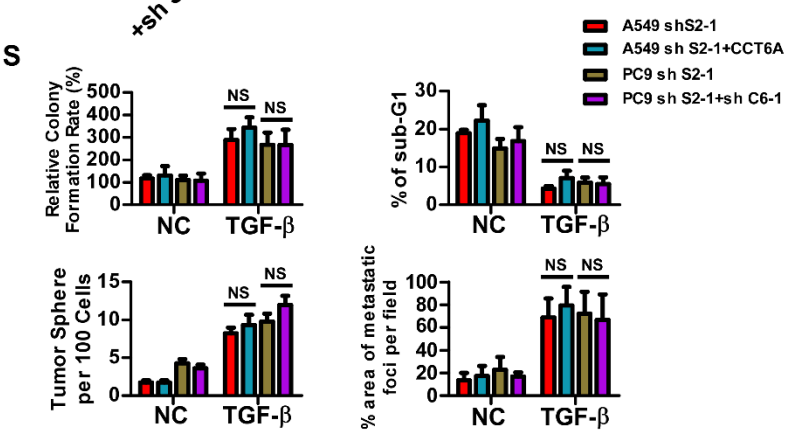

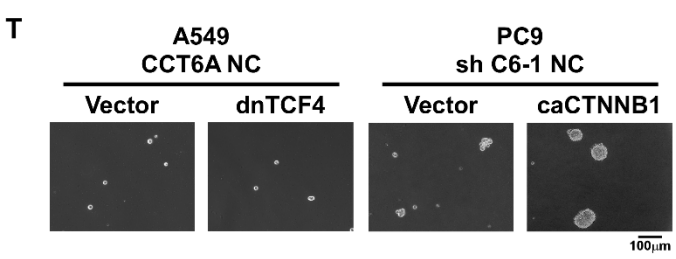

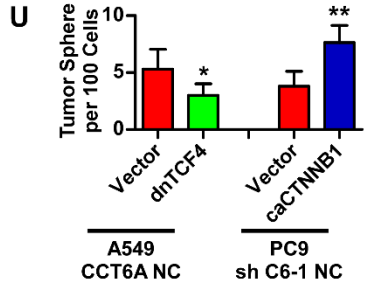

Supplementary Figure S6. CCT6A mediates TGF-β-promoted metastasis of NSCLC cells.

(A-K) Luciferase living image of mice at different time points following intravenously (via tail vein) injecting indicated NSCLC cells (A) and the mice living image of day 30 are also shown in Figure 6 A and C. Kaplan-Meier survival analysis of mice intravenously (via tail vein) injected with indicated NSCLC cells (B). Luciferase live-cell imaging (C and G), picric acid staining of metastatic nodes and H&E staining of lung tissue (D and H), area percentage of tumor metastatic foci per field (E and I) and Kaplan-Meier survival analysis (F and J) of mice with intravenously (via tail vein) injected the indicated NSCLC cells (CCT6A shRNA set2 and SMAD2 shRNA). Representative images were from 2 independent experiments with 6 mice per group with similar results. Error bars represent the means ± SD of 3 independent experiments. *P* values were obtained from ANOVA with Dunnett's *t*-test, $^{**}P < 0.01$. Scale bar: 100 μm. (K) Immunohistochemical staining of p-SMAD2 and p-SMAD3 proteins in paraffin sections of the indicated xenografts. Scale bar: 100 μm. **(L-N)** Luciferase living image of mice at different time points following subcutaneously injecting indicated NSCLC cells into inguinal folds (L) and the mice living image of day 40 are also shown in Figure 6 E and G. The area percentage of tumor metastatic foci per field (M) and Kaplan-Meier survival analysis (N) of mice subcutaneously injected with indicated NSCLC cells into inguinal folds. Representative images were from 2 independent experiments with 6 mice per group with similar results. *P* values were obtained by performing ANOVA with Dunnett's *t*-test, $^{**}P < 0.01$. **(O-Q)** Luciferase live-cell imaging (O), picric acid staining of metastatic foci (P) and Kaplan-Meier survival analysis (Q) of C57BL/6 mice intravenously (via tail vein) injected with indicated LLC cells. Representative images were from 2 independent experiments with 6 mice per group with similar results. **(R, S)** Comparison of the biological outcomes between groups with SMAD2 knocked down alone and with SMAD2 knocked down plus CCT6A overexpression or knockdown. Kaplan-Meier survival analysis of mice intravenously (via tail vein) injected with indicated NSCLC cells (R) and statistical analyses of colony formation in an adherent culture, tumor sphere formation, sub-G1 DNA content of detached cells and the area percentages of tumor metastatic foci per field were performed in indicated cells (S). Error bars represent means ± SD of 3 independent experiments. *P* values were obtained by performing ANOVA with Dunnett's *t*-test, NS: $P > 0.05$. **(T, U)** Tumor sphere formation assays with indicated NSCLC cells. Error bars represent the means ± SD, *P* values were obtained from Student's *t* test, $^{*}P < 0.05$, $^{**}P < 0.01$.